ISSN 1029-9599, Physical Mesomechanics, 2024, Vol. 27, No. 4, pp. 398–408. © Pleiades Publishing, Ltd., 2024.
Russian Text © The Author(s), 2024, published in Fizicheskaya Mezomekhanika, 2024, Vol. 27, No. 2, pp. 81–92.

Influence of Heat Treatments on Martensitic Transformations and Elastocaloric Effect in Two-Phase (β + γ) NiFeGa Alloys

I. D. Kurlevskaya[1]*, E. Yu. Panchenko[1], A. B. Tokhmetova[1], E. I. Yanushonite[1], A. S. Eftifeeva[1], N. Yu. Surikov[1], E. E. Timofeeva[1], and Yu. I. Chumlyakov[1]

[1] *National Research Tomsk State University, Tomsk, 634050 Russia*
** e-mail: kurl.irina@yandex.ru*

Received July 10, 2023; revised September 11, 2023; accepted September 25, 2023

Abstract—This study reveals the impact of the formation mechanism of a two-phase (β + γ) structure during heat treatment on thermoelastic $L2_1$(B2)-10M/14M-$L1_0$ martensitic transformations and elastocaloric parameters of polycrystalline $Ni_{54}Fe_{19}Ga_{27}$ alloy. It is experimentally shown that annealing of the as-cast $Ni_{54}Fe_{19}Ga_{27}$ alloy in the temperature range 1173–1463 K for 0.5 h followed by water quenching leads to the precipitation of the γ phase at grain boundaries and inside grains. As the annealing temperature increases from 1173 to 1463 K, the thickness of the γ-phase layer at the grain boundaries doubles, particles inside the grains coarsen, and their volume distribution becomes nonuniform. Simultaneously, the martensitic transformation temperatures increase by 31–69 K. The nonuniform distribution of the γ-phase particles and the morphological features of martensite (refinement of its twinned structure) lead to a 5–6-fold widening of the martensitic transformation intervals in crystals annealed at 1448 K compared to the as-cast alloy. After cyclic superelastic tests with 20 to 100 loading/unloading cycles, two-phase (β + γ) polycrystals demonstrate the stable adiabatic cooling temperature ΔT_{ad} (2.7–3.0 K) and do not crack along grain boundaries, unlike those in the as-cast state. Significant fatigue strength and a high coefficient of performance (up to 18.3) make (β + γ) $Ni_{54}Fe_{19}Ga_{27}$ polycrystals promising for practical use in solid-state cooling.

Keywords: shape memory alloys, martensitic transformations, heat treatment, superelasticity, elastocaloric effect

DOI: 10.1134/S1029959924040040

1. INTRODUCTION

An urgent need to develop new materials for environmentally friendly and high performance solid-state cooling systems has arisen due to the adverse environmental impact of refrigerants used in vapor compression refrigeration systems. One of the most promising technologies is based on the elastocaloric effect [1]. This effect manifests itself in loading/unloading cycles of shape memory alloys, which, thanks to thermoelastic martensitic transformations and significant reversible strains, have already proven themselves to be effective functional materials used in actuators and sensors, medical tools and implants. Elastocaloric cooling is observed in the temperature range of superelasticity and is based on a decrease in the material temperature during reverse martensitic transformations under adiabatic conditions. Important requirements for elastocaloric materials are a high cooling capacity, a wide range of operating temperatures, and cyclic stability of superelastic and elastocaloric parameters [2]. This ensures the durability and high performance of solid-state cooling systems. Despite numerous studies on the elastocaloric effect of a number of alloys (CuZnAl, NiTi, CoNiGa, and CoNiAl) [2–4], the development of materials with the most favorable combination of these parameters is still relevant.

Ferromagnetic NiFeGa alloys, which undergo thermoelastic $L2_1$(B2)-10M/14M-$L1_0$ martensitic transformations, are considered high on the list of candidates for solid-state cooling. When the shape memory effect and superelasticity manifest themselves, these alloys experience significant reversible strains close to theoretical ones (+13.5% in tension and –6.2% in compression) [5, 6]. Unlike NiTi with a narrow temperature range of the elastocaloric effect (~50 K), NiFeGa single crystals are characterized by the stable adiabatic cooling temperature ΔT_{ad} = 6–13 K [2, 7–9] in the entire temperature range of superelasticity, reaching 200 K under compression.

Practical application of single crystals presents a problem because of the complexity and high cost of their production, while the production of polycrystalline materials is more cost-efficient. The main obstacle to their use is brittle fracture at grain boundaries on account of the incompatibility of strains in neighboring grains during transformation [1]. Different orientations of grains with respect to external loading and a strong orientation dependence of strain during stress-induced martensitic transformations are key factors in stress concentration and grain boundary cracking of the material. One of the ways to increase the plasticity is to eliminate triple junctions of grains by forming an oligocrystalline structure [10], which increases the reversibility of martensitic transformations and makes the superelastic characteristics closer to those of single crystals, as shown by an example of CuAlNi wires [11]. In [12, 13], grain boundary cracking of polycrystalline NiMnGa and CuZnAl alloys was reduced by grain refinement and strengthening of grain boundaries by such elements as Zr, Ti, B, V, Cr, and Gd. Finally, the resistance of polycrystals to fracture can be increased by forming a layer of the ductile γ phase along grain boundaries. It was shown that the two-phase (β + γ) structure significantly improved the plasticity and fatigue resistance of the material [1, 14, 15]. The distribution of second-phase particles along grain boundaries and inside grains, their size and volume fraction affect martensitic transformations and depend on the heat treatment mode required to obtain a two-phase (β + γ) structure of the alloy. However, the previous investigations of NiFeGa polycrystals were carried out after the only possible heat treatment mode, and no dependence of the functional properties on the resulting microstructural parameters was found. Therefore, this work is devoted to the formation of a two-phase (β + γ) structure during heat treatment and its influence on thermoelastic martensitic transformations and the elastocaloric effect in polycrystalline $Ni_{54}Fe_{19}Ga_{27}$ alloy.

2. EXPERIMENTAL PROCEDURE

Polycrystals of ferromagnetic $Ni_{54}Fe_{19}Ga_{27}$ alloy (at %) were obtained by arc melting in an argon atmosphere. A cylindrical ingot 9 cm long and 1.2 cm in diameter was obtained upon crystallization. Along the ingot edge, where the cooling rate was the highest, a narrow region with numerous fine grains was formed. The main volume consisted of long columnar grains directed towards the center, which formed parallel to the heat flow direction during cooling. Their length ranged from 0.3 to 4.0 mm, and the average transverse size was 100–170 μm. Compression specimens were spark cut out of the ingot, outside the edge area, in the shape of a rectangular parallelepiped with the dimensions $3 \times 3 \times 6$ mm^3. The loading axis of the specimens was chosen parallel to the longitudinal axis of the ingot, and consequently grains were elongated perpendicular to the loading axis of the specimen. Before testing, the specimens were ground and electrolytically polished. To study the influence of the heat treatment mode on martensitic transformations and the elastocaloric effect, we used as-cast polycrystals and those water quenched after high-temperature annealing for 0.5 h at different temperatures: 1173, 1273, 1423, 1448, and 1463 K. These annealing temperatures correspond to the two-phase (β + γ) field in the phase diagram of the $Ni_{54}Fe_{19}Ga_{27}$ alloy [16].

The surface microstructure of the polycrystalline $Ni_{54}Fe_{19}Ga_{27}$ alloy was studied by optical metallography using a Keyence VHX-2000 microscope. The volume fraction of the γ phase was determined using the software embedded in the Keyence VHX-2000 microscope. The elemental composition of the polycrystals was analyzed by energy-dispersive X-ray spectroscopy on a TESCAN VEGA 3 scanning electron microscope. The phase composition of the specimens was determined by X-ray diffraction analysis at room temperature on a Shimadzu XRD 6000 X-ray diffractometer (CuKα radiation). Diffraction patterns were interpreted using the PowderCell 2.4 program. Thermal characteristics and temperatures of martensitic transformations (start and finish temperatures of direct (M_s and M_f) and reverse (A_s and A_f) transformations) were calculated during cooling/heating in a free state from the temperature dependence of heat flow by differential scanning calorimetry using a NETZSCH DSC 404 F1 calorimeter at the heating/cooling rate 10 K/min. The error for the characteristic martensitic transformation temperatures was 2 K. Superelastic tests were carried out on an Instron 5969 electromechanical testing machine with the stress error ±2 MPa. The microstructure of the polycrystals was studied using a Hitachi HT-7700 transmission electron microscope. Thin foils for microscopy were prepared by jet polishing using a Tenupol-5 installation.

The adiabatic cooling temperature ΔT_{ad} was determined under superelastic conditions by measuring the specimen temperature with a highly sensitive T-type thermocouple. To register the elastocaloric ef-

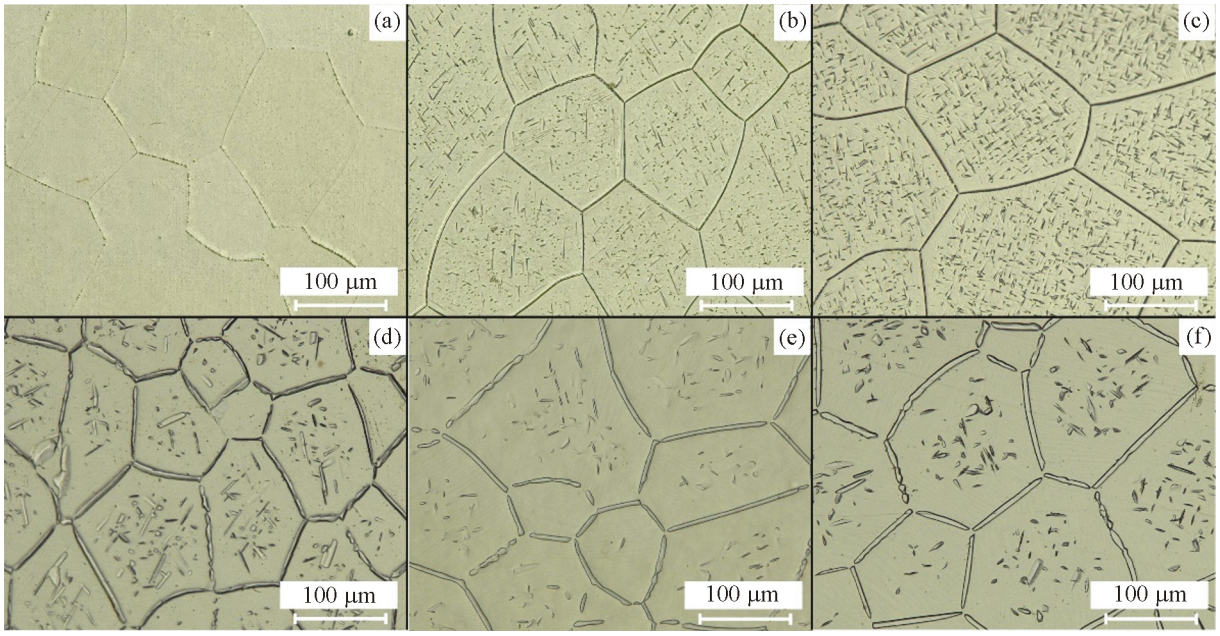

Fig. 1. Optical metallography of the surface of polycrystalline $Ni_{54}Fe_{19}Ga_{27}$ alloy in the as-cast state (a) and after annealing for 0.5 h followed by quenching at 1173 (b), 1273 (c), 1423 (d), 1448 (e), and 1463 K (f) (color online).

fect, the specimen was loaded at a low strain rate of 2.0×10^{-3} s^{-1} to the given stress and then held at this level for 6 s to equalize the specimen temperature with the test temperature. For a closer approximation to adiabatic conditions, unloading was carried out at a high strain rate of 6.7×10^{-1} s^{-1}. The time dependence of the specimen temperature was recorded using a data acquisition module consistently in time with the σ(ε) curves. The error for ΔT_{ad} was 0.5 K.

3. RESULTS AND DISCUSSION

Figure 1 presents the results of optical metallography of the surface of polycrystalline $Ni_{54}Fe_{19}Ga_{27}$ alloy in the as-cast state and after heat treatments. The results of X-ray diffraction and transmission electron microscopy of the polycrystalline $Ni_{54}Fe_{19}Ga_{27}$ alloy in the as-cast state are shown in Figs. 2a and 3, respectively. It is shown that, after melting at room temperature, the polycrystals are in the high-temperature

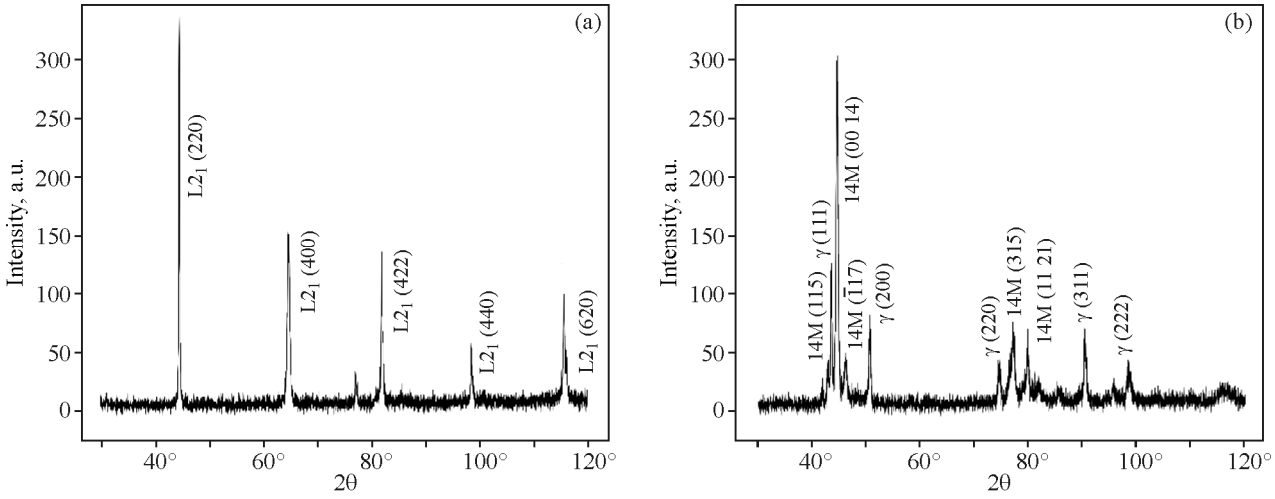

Fig. 2. X-ray diffraction patterns of polycrystalline $Ni_{54}Fe_{19}Ga_{27}$ alloy in the as-cast state (a) and after annealing at $T = 1448$ K for 0.5 h followed by water quenching (b).

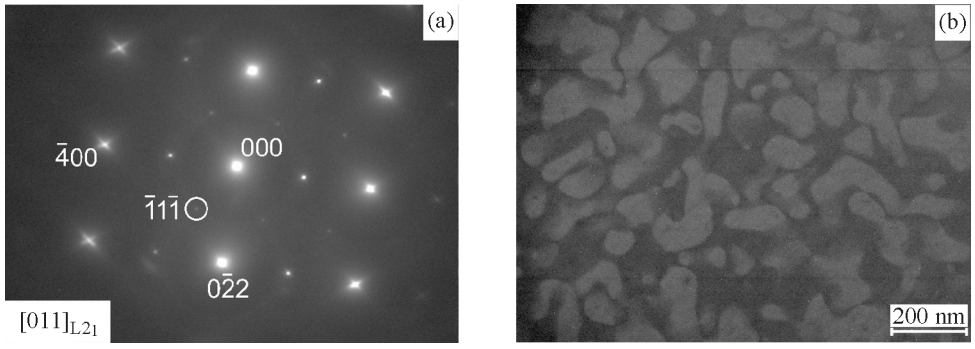

Fig. 3. Microstructure of polycrystalline $Ni_{54}Fe_{19}Ga_{27}$ alloy in the as-cast state: SAED pattern of $L2_1$ austenite, axis of the $[011]_{L2_1}$ zone (a), and dark-field image in the superstructural {111} reflection demonstrating antiphase domains (b).

β phase (Figs. 1a, 2a). No γ-phase peaks are observed in the X-ray diffraction pattern (Fig. 2a). Superstructural {111} reflections detected in the SAED patterns point to the $L2_1$ structure of the high-temperature β phase with the lattice parameter 0.576 nm (Fig. 3a). It is known [17] that superstructural reflections for which, according to the extinction rules, the following condition is satisfied: h, k, l are odd, and $h+k+l=2n+1$ ({111}, {311} and {331} reflections), are absent in the B2 structure. As can be seen from Fig. 1a, there is a small volume fraction of fine oxide particles along grain boundaries and inside grains, which were formed during melting. It is assumed that these particles do not have a significant effect on the material properties [18].

High-temperature heat treatments lead to the formation of a two-phase (β + γ) structure (Figs. 1b–1f). After annealing at $T=1173$ and 1273 K followed by water quenching, the second phase is precipitated along grain boundaries in the form of a continuous thin layer 2–3 μm thick and numerous fine particles up to ~30 μm long inside grains (Figs. 1b, 1c). With treatment temperature (1423, 1448, and 1463 K), the structure changes. Instead of a continuous layer, individual elongated particles up to 6 μm in thickness are formed along grain boundaries, thus certain boundary sections are free of the γ phase. Grains smaller than 90–100 μm are free of particles. The maximum particle length reaches 60 μm, while their number inside grains decreases (Figs. 1d–1f).

Figure 2b shows an X-ray diffraction pattern of the polycrystal after high-temperature annealing at $T=1448$ K for 0.5 h followed by water quenching. It is seen that the heat treatment results in the formation of γ-phase particles characterized by a face-centered cubic (fcc) lattice with the parameter 0.36 nm. Along with the γ-phase peaks, the X-ray diffraction pattern has peaks corresponding to a monoclinic structure with the parameters $a=0.4204$ nm, $b=0.2697$ nm, $c=2.8963$ nm, and $\beta=85.27°$, which, according to [19], corresponds to layered modulated 14M martensite. The presence of the 14M martensite peaks indicates an increase in the characteristic martensite start temperature in the annealed state. It is known [5] that 14M martensite is an intermediate structure, and, upon further cooling and/or under loading, the $Ni_{54}Fe_{19}Ga_{27}$ alloy structure transforms into tetragonal $L1_0$ martensite.

The elemental analysis of the $Ni_{54}Fe_{19}Ga_{27}$ polycrystals after high-temperature heat treatments shows that the composition of the matrix is close to the nominal one (Table 1).

Figure 4 shows SEM images of the surface of $Ni_{54}Fe_{19}Ga_{27}$ polycrystals annealed at $T=1273$ and 1423 K and the results of elemental analysis when scanning along a line intersecting the grain boundary

Table 1. Results of elemental analysis of $Ni_{54}Fe_{19}Ga_{27}$ polycrystals after annealing at $T=1273$ K for 0.5 h followed by water quenching

	Chemical composition, at %		
	Ni	Fe	Ga
Matrix	54.7 ± 0.5	18.4 ± 0.2	26.9 ± 0.7
Grain boundary γ phase	54.4 ± 1.5	25.3 ± 0.3	20.3 ± 1.7
γ-phase particles inside a grain	53.4 ± 0.9	24.7 ± 1.5	21.9 ± 2.2

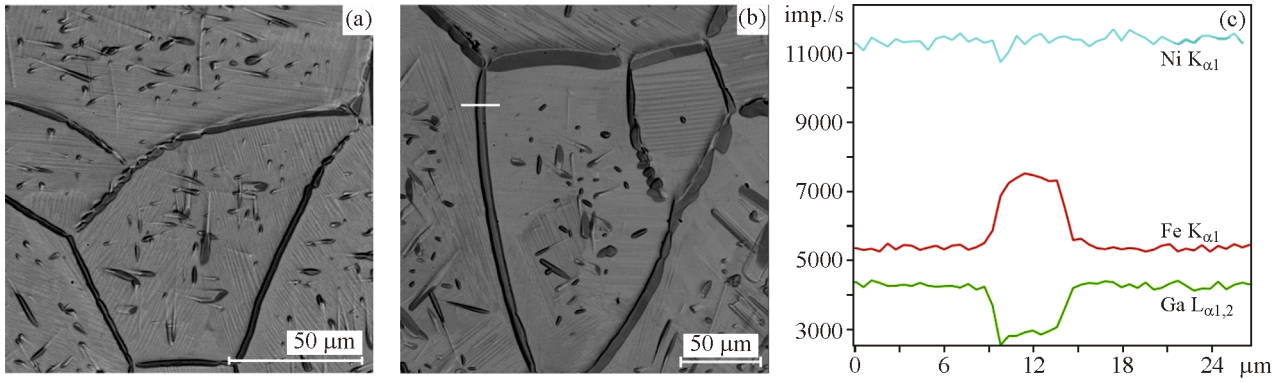

Fig. 4. SEM image of the surface of $Ni_{54}Fe_{19}Ga_{27}$ polycrystals after annealing at $T = 1273$ K for 0.5 h (a) and at $T = 1423$ K for 0.5 h (b) with elemental analysis of the surface along the line indicated in (b) through the grain boundary γ-phase interlayer (c) (color online).

γ-phase interlayer. It can be seen that the γ-phase precipitate is enriched in Fe and depleted of Ga compared to the matrix, which is also consistent with the data from Table 1 for the alloy annealed at $T = 1273$ K for 0.5 h. Similar relations between the chemical compositions of the matrix and the γ phase of NiFeGa alloys were deduced in [6, 14, 16].

The dependence of the martensitic transformation temperatures on the heat treatment temperature in $Ni_{54}Fe_{19}Ga_{27}$ polycrystals is shown in Fig. 5. The as-cast polycrystals are characterized by the martensitic transformation temperatures $M_s = 284$ K and $A_f = 296$ K. Annealing at $T = 1173$ K for 0.5 h leads to a decrease in the temperatures ($M_s = 259$ K and $A_f = 269$ K) compared to the as-cast alloy.

Two intervals can be distinguished in the dependence of the start and finish temperatures of direct M_s and reverse martensitic transformations A_f on the annealing temperature. In the first interval from 1173 to

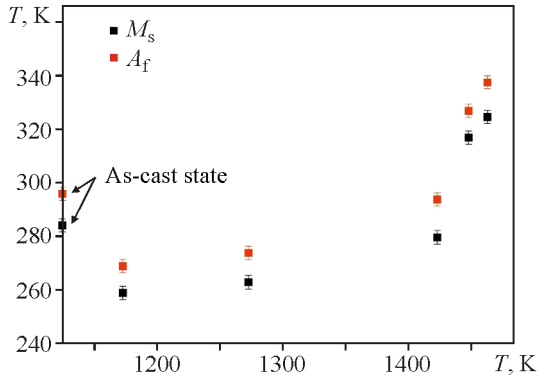

Fig. 5. Martensitic transformation temperatures (M_s, A_f) depending on the annealing temperature for $Ni_{54}Fe_{19}Ga_{27}$ polycrystals (color online).

1423 K, the martensitic transformation temperatures gradually increase, approaching the values of the as-cast alloy. With a further increase in the annealing temperature (the second interval from 1423 to 1463 K), the martensitic transformation temperatures sharply increase, so that they exceed the values of the as-cast alloy ($M_s = 284$ K, $A_f = 296$ K, and $M_s = 325$ K, $A_f = 338$ K after annealing at $T = 1463$ K).

Further investigation of thermal characteristics, superelastic and elastocaloric parameters was performed on polycrystals in the three structural states: after arc melting (state I) and after annealing at $T = 1273$ K (state II) and $T = 1448$ K (state III) for 0.5 h followed by water quenching. These treatment temperatures were chosen because they lie in the central part of each of the two temperature intervals (1173–1423 and 1423–1463 K). For states II and III, the volume fraction of the γ phase located both inside grains and along boundaries is 18 and 24%, respectively. Figure 6 shows calorimetric curves for direct and reverse martensitic transformations.

State I is characterized by sharp and narrow peaks of heat release and absorption during martensitic transformations in the cooling/heating cycle. When cooled in a free state, martensite is twinned in the grain, so that large lamellae pass through the grain, inducing high internal stresses at its boundaries (Fig. 7).

As can be seen from Table 2, the second-phase precipitation in states II and III causes the temperature ranges of direct $\Delta_1 = M_s - M_f$ and reverse $\Delta_2 = A_s - A_f$ martensitic transformations to widen (from 8 K in state I to 13 K in state II). In state III, Δ_1 and Δ_2 enlarge by 5–6 times compared to those in state I and amount to 38–50 K.

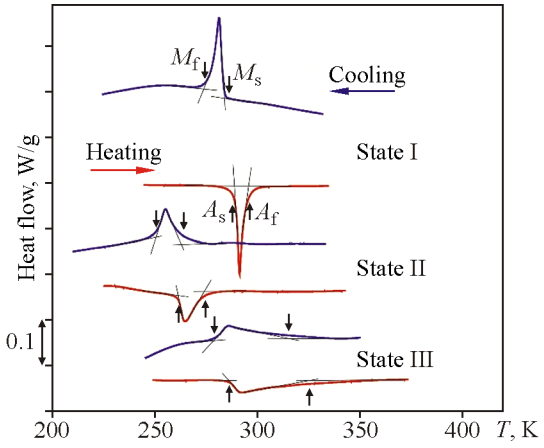

Fig. 6. Differential scanning calorimetry curves obtained during cooling/heating for $Ni_{54}Fe_{19}Ga_{27}$ polycrystals: in the as-cast state (state I), after annealing for 0.5 h at T = 1273 (state II) and 1448 K (state III) (color online).

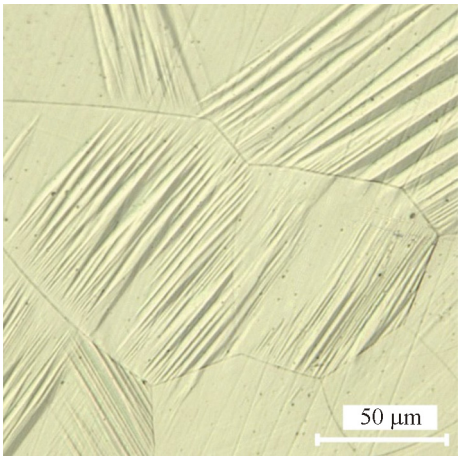

Fig. 7. Optical metallography of the surface of polycrystalline $Ni_{54}Fe_{19}Ga_{27}$ alloy in the as-cast state at a temperature below M_f (color online).

Thermodynamic analysis of martensitic transformations reveals that the temperature ranges of direct and reverse transformations Δ_1 and Δ_2 characterize the elastic and surface energy $|\Delta G_{rev}(1)|$ accumulated in the material during martensitic transformations [20, 21]:

$$\left|\Delta G_{rev}(1)\right| = (\Delta_1 + \Delta_2)\frac{\Delta S}{2}, \qquad (1)$$

where ΔS is the change in entropy during transformation.

Thus, widening of Δ_1 and Δ_2 in the two-phase polycrystals (states II and III) compared to the single-phase ones (state I) is associated with an increase in the elastic and surface energy due to the presence of particles that do not undergo martensitic transformations. Much wider temperature ranges of direct and reverse martensitic transformations in states II and III are also explained by the morphology of the resulting martensite. Upon cooling of the two-phase ($\beta+\gamma$) crystals, various types of finely dispersed martensite form in the same grain (Figs. 4a, 4b), in contrast to large martensite lamellae passing through the grain of the as-cast polycrystals (state I) (Fig. 7). This leads to an increase in the density of twin boundaries in martensite, provides a better elastic accommodation of deformation during transformation for misoriented grains, and increases the elastic and surface energy $|\Delta G_{rev}(1)|$ accumulated in the state II and III alloys during martensitic transformations.

The wide temperature ranges Δ_1 and Δ_2 in state III (38–50 K) can be also contributed by the inhomogeneous structure of the material: γ-phase particles are undetected both in fine grains and along boundaries of coarse grains at a distance of ~50 μm. This can lead to martensitic transformations in zones with different microstructures in different temperature ranges.

Despite the enlargement of the temperature intervals Δ_1 and Δ_2, the hysteresis value $\Delta T = A_f - M_s$ remains almost unchanged for all three states (ΔT = 12 K (state I), 11 K (state II), 10 K (state III)). It is known that the temperature hysteresis determines the energy dissipation in the cycle during martensitic transformations [20, 21]:

$$\left|\Delta G_{fr}\right| = \frac{\Delta S_{ch}}{2}(A_f - M_s). \qquad (2)$$

From the obtained data (Fig. 5, Table 2), it follows that, in crystals with a ($\beta+\gamma$) structure, energy dissi-

Table 2. Temperatures of martensitic transformations, temperature intervals, and thermal hysteresis in $Ni_{54}Fe_{19}Ga_{27}$ polycrystals in the three states

State	M_s, K	M_f, K	A_s, K	A_f, K	Δ_1, K	Δ_2, K	ΔT, K
As-cast (I)	284	276	288	296	8	8	12
1273 K, 0.5 h (II)	263	250	261	274	13	13	11
1448 K, 0.5 h (III)	317	279	277	327	38	50	10

Table 3. Thermal characteristics of $Ni_{54}Fe_{19}Ga_{27}$ polycrystals in the three states

State	C_p, J/(kg K)	ΔS^{A-M}, J/(kg K)	ΔS^{M-A}, J/(kg K)	ΔT_{ad}^t, K
As-cast (I)	455	16.8	15.9	10.1
1273 K, 0.5 h (II)	444	15	11.9	7.2
1448 K, 0.5 h (III)	505	12.8	11.1	7.1

pation during reversible martensitic transformations does not increase compared to the state I alloy, which should contribute to the cyclic stability of functional properties of the material, including elastocaloric cooling, regardless of the structural state.

The change in entropy during direct ΔS^{A-M} and reverse ΔS^{M-A} martensitic transformations was determined using differential scanning calorimetry (Table 3). Since not the entire volume of the material experiences martensitic transformations in the two-phase structure, ΔS during both direct and reverse martensitic transformations in the state II and III alloys decreases compared to the state I alloy. The specific heat capacity C_p for state I is $C_p = 455$ J/(kg K). In state II characterized by numerous fine particles in grains, C_p decreases by 11 J/(kg K). A similar decrease in the heat capacity is demonstrated by $Ni_{54}Fe_{19}Ga_{27}$ single crystals annealed at 1373 K for 0.5 h, in which 5–35 μm particles precipitate, as shown in [7]. In state III, the heat capacity increases to 505 J/(kg K).

The experimental values for the entropy change during reverse martensitic transformations ΔS^{M-A} and the specific heat capacity C_p can be used to find the theoretical resource of adiabatic cooling of the material [2]:

$$\Delta T_{ad}^t = \frac{T_0 \Delta S^{M-A}}{C_p}, \qquad (3)$$

where $T_0 \approx (M_s + A_f)/2$ is the temperature of chemical equilibrium of the austenitic and martensitic phases.

The theoretical temperature of adiabatic cooling ΔT_{ad}^t derived by this formula for state I is 10.1 K. For two-phase ($\beta + \gamma$) structures (state II and III), the theoretical temperature is lower: 7.2 and 7.1 K, respectively.

The investigation of superelasticity of $Ni_{54}Fe_{19}Ga_{27}$ polycrystals in states I and II is carried out at the temperature 323 K. Since this temperature for state III is below $A_f = 327$ K, and consequently the shape memory effect appears in the loading/unloading cycle, superelastic parameters in state III are studied at 348 K. All three states are characterized by low critical stresses of martensite formation σ_{cr} (150–200 MPa). In the first loading/unloading cycle, irreversible strain 0.5–0.9% accumulates (Fig. 8). This may be due to the fact that the main processes of stress relaxation and plastic deformation occur along the boundaries of grains with the greatest incompatibility of strains during martensitic transformations. In subsequent, quite stable and almost completely reversible, cycles of loading to the same strain, the critical stresses σ_{cr} decrease by 12 MPa in state I, by 10 MPa in state II, and by 53 MPa in state III from those in the first cycle. A strong decrease in σ_{cr} in state III may be due to significant plastic deformation of the

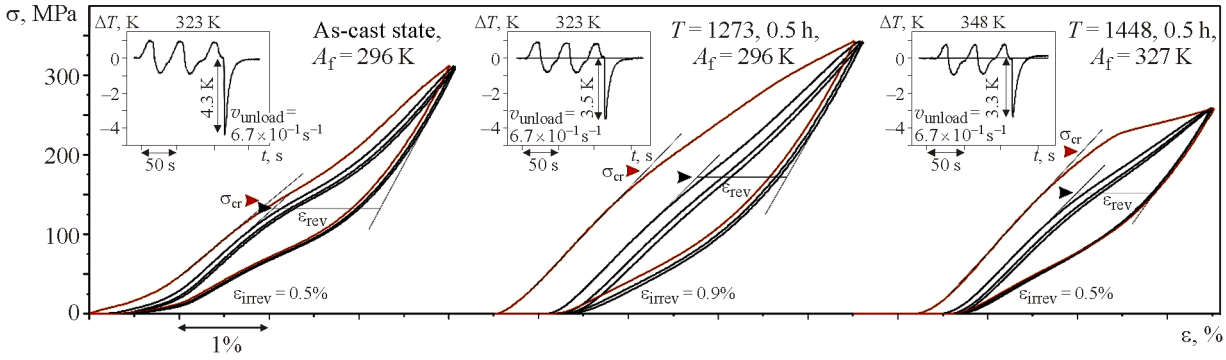

Fig. 8. Dependences σ(|ε|) and the corresponding time dependences of the specimen temperature (inset) when studying the superelastic and elastocaloric effects in polycrystalline $Ni_{54}Fe_{19}Ga_{27}$ alloy in various structural states (color online).

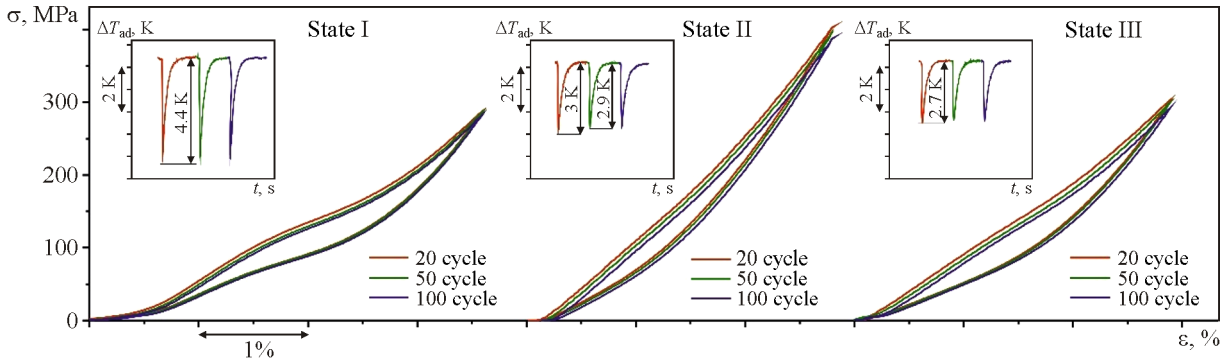

Fig. 9. Superelastic σ(ε) curves and the corresponding curves of the specimen temperature on the cycle number (inset) revealing the elastocaloric effect in polycrystalline $Ni_{54}Fe_{19}Ga_{27}$ alloy (color online).

thick γ-phase layer along grain boundaries, as well as due to coarse particles in grains.

The investigation of the elastocaloric effect in the fourth cycle shows that, in state I, the adiabatic cooling temperature is $\Delta T_{ad} = 4.3$ K, which is comparable to the literature data for single-phase $Ni_{54}Fe_{19}Ga_{27}$ polycrystals [1]. For states II and III, $\Delta T_{ad} = 3.5$ K and 3.3 K, respectively. The decrease in the experimental values of ΔT_{ad} in two-phase polycrystals corresponds to a decrease in the theoretical resource ΔT_{ad}^{t} (Table 3). This is due to the fact that γ-phase particles do not undergo martensitic transformations, i.e. not the entire volume of the material participates in the transformation, which reduces thermal effects. The experimental values of the elastocaloric effect are lower than the calculated ones due to the fact that the experimental conditions are not purely adiabatic due to the finite rate of unloading and heat exchange with the grips of the testing machine. In addition, the first cycles of superelasticity are characterized by significant irreversible strain, stabilization of stress-assisted martensite in deformed regions, and a reduced volume fraction of the material subjected to stress-assisted martensitic transformations in subsequent cycles.

The first requirement for materials that can be used in solid-state cooling is cyclic stability of their functional properties. The cyclic stability of superelastic and elastocaloric parameters of $Ni_{54}Fe_{19}Ga_{27}$ polycrystals was studied in 100 loading/unloading cycles at 323 K in states I and II and at 348 K in state III (Fig. 9). The test load was set in such a way that the σ(|ε|) curve was completely reversible in the second (third) cycle.

The second important requirement is high performance of elastocaloric cooling in the loading/unloading cycle, the most common measure for which is the coefficient of performance (COP). It is defined as the ratio of the useful energy absorbed by a specimen from the environment during an endothermic reaction to the amount of energy dissipated in the thermodynamic cycle [22]:

$$\mathrm{COP} = \frac{C_p \Delta T_{ad}}{1/\rho \oint \sigma d\varepsilon}, \qquad (4)$$

where ρ is the material density ($\rho = 8450$ kg/m^3 for $Ni_{54}Fe_{19}Ga_{27}$ [23]).

The σ(ε) dependence for the studied states becomes stable starting from the 20th cycle (Fig. 9). The shape of the curve for the as-cast polycrystals resembles typical superelastic curves for single crystals and is characterized by critical stresses of start of martensitic transformation $\sigma_{cr} = 121$ MPa and reversible strain ~1%. The value of the elastocaloric effect is $\Delta T_{ad} = 4.4$ K, and COP = 23.3. These values do not change throughout all 100 cycles.

In two-phase (β + γ) states, the behavior of the σ(ε) dependence changes: the strain hardening coefficient increases during stress-assisted martensitic transformation, the plateau of martensitic transformation disappears, and reversible strain decreases. In cyclic tests, the stable adiabatic cooling temperature is lower than those measured in the fourth cycle: by the 20th cycle, ΔT_{ad} decreases to 2.9–3.0 and to 2.7 K in states II and III, respectively, after which it remains unchanged. This is due to stabilization of a part of the martensite in the first cycles, which makes no contribution to the thermal effect during subsequent loading/unloading cycles, i.e. the material volume subjected to martensitic transformation is further reduced. The COP is 18.3 for state II and 17.1 for state III. Due to the low energy dissipation in the loading/unloading cycle, the COPs in the two-phase states with better plasticity exceed the values previ-

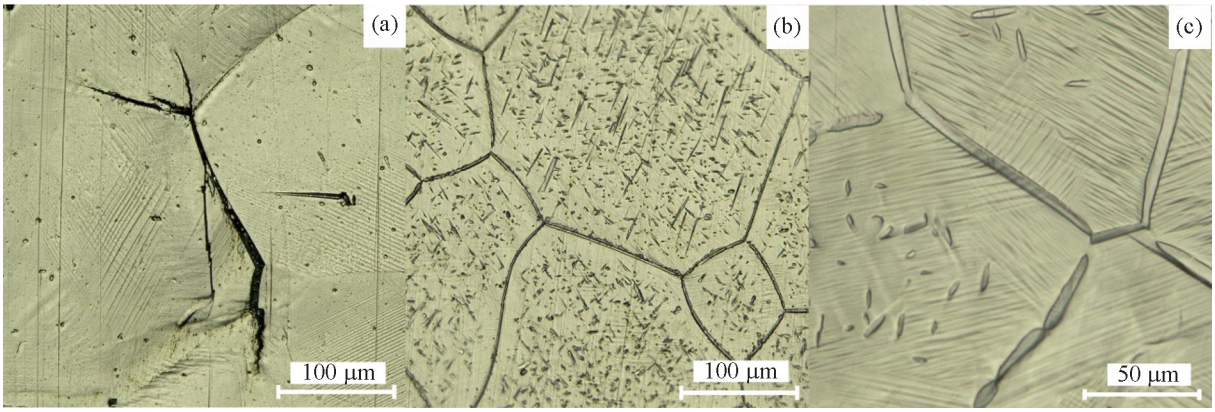

Fig. 10. Microstructure of polycrystalline $Ni_{54}Fe_{19}Ga_{27}$ alloy in state I (a), II (b), and III (c) after cyclic superelastic and elastocaloric tests (color online).

ously obtained for polycrystalline and single-crystal NiFeGa(Co) alloys [7, 15, 24].

The structure of specimens tested in 100 cycles is shown in Fig. 10. Cyclic tests on the state I polycrystals with the highest adiabatic cooling temperatures (4.4 K) and COP (23.3) reveal multiple grain boundary cracking as well as traces of plastic deformation (Fig. 10a). This is explained by high internal stresses induced by the incompatibility of strains during stress-assisted transformation due to the growth of large martensite lamellae (Fig. 7). In states II and III, due to elastic and plastic deformation of the grain boundary γ-phase layer during loading/unloading, no fracture occurs along grain boundaries (Figs. 10b, 10c). In addition, the resistance of the two-phase polycrystals to fracture increases as a result of the growth of fine crystals of various martensite in the same grain.

4. CONCLUSIONS

The formation of a two-phase (β + γ) structure and its influence on thermoelastic martensitic transformations and the elastocaloric effect were studied on polycrystalline $Ni_{54}Fe_{19}Ga_{27}$ alloy subjected to different heat treatments. The results obtained suggest the following conclusions.

Annealing of $Ni_{54}Fe_{19}Ga_{27}$ polycrystals at 1173–1463 K for 0.5 h followed by water quenching caused the formation of a two-phase (β + γ) structure: particles of the plastic γ phase precipitated both along grain boundaries and inside grains. When the annealing temperature increased from 1173 to 1463 K, cracks appeared in the grain boundary γ-phase interlayer, and its thickness increased from 2 to 6 μm. Particles inside grains coarsened, and their distribution became nonuniform.

A rise in the annealing temperature from 1173 to 1463 K contributed to an increase in the characteristic martensitic transformation temperatures by 31–69 K. The formation of the γ phase increased the accumulated elastic and surface energy during martensitic transformations, which, along with changes in the martensite morphology, widened in the temperature ranges of martensitic transformations at a constant hysteresis ΔT in two-phase (β + γ) polycrystals of the $Ni_{54}Fe_{19}Ga_{27}$ alloy.

The formation of a ductile γ-phase interlayer at grain boundaries improved the plasticity and fatigue strength of the material compared to the single-phase state due to compatibility of transformation strain at the boundary during martensitic transformations and reduced stress gradient. High fatigue strength and high COPs (17.1 and 18.3, respectively) make two-phase (β + γ) polycrystals of $Ni_{54}Fe_{19}Ga_{27}$ alloy promising for use in solid-state cooling at the adiabatic cooling temperature ΔT_{ad} up to 3 K in the operating cycle.

To optimize the two-phase state of NiFeGa alloys and to use a more complete theoretical resource of adiabatic cooling ΔT_{ad}^{t}, it is necessary to form a thin layer of the plastic γ phase along grain boundaries no thicker than 2–3 μm as well as to reduce the size and volume fraction of particles inside grains to increase the material volume undergoing martensitic transformations.

ACKNOWLEDGMENTS

The microstructure of polycrystals was studied using a Hitachi HT-7700 transmission electron micro-

scope at the Krasnoyarsk Regional Collective Use Center of the Federal Research Center KSC SB RAS.

FUNDING

The study was supported by Russian Science Foundation grant No. 23-19-00150, https://rscf.ru/project/23-19-00150/.

CONFLICT OF INTEREST

The authors of this work declare that they have no conflicts of interest.

REFERENCES

1. Xu, Y., Lu, B., Sun, W., Yan, A., and Liu, J., Large and Reversible Elastocaloric Effect in Dual-Phase $Ni_{54}Fe_{19}Ga_{27}$ Superelastic Alloys, *Appl. Phys. Lett*., 2015, vol. 106, p. 201903. https://doi.org/10.1063/1.4921531
2. Wu, Y., Ertekin, E., and Sehitoglu, H., Elastocaloric Cooling Capacity of Shape Memory Alloys. Role of Deformation Temperatures, Mechanical Cycling, Stress Hysteresis and Inhomogeneity of Transformation, *Acta Mater*., 2017, vol. 135, pp. 158–176. https://doi.org/10.1016/j.actamat.2017.06.012
3. Shen, A., Zhao, D., Sun, W., Liu, J., and Li, C., Elastocaloric Effect in $Co_{50}Ni_{20}Ga_{30}$ Single Crystal, *Scripta Mater*., 2017, vol. 127, pp. 1–5. https://doi.org/10.1016/j.scriptamat.2016.08.030
4. Pataky, G., Ertekin, E., and Sehitoglu, H., Elastocaloric Cooling Potential of NiTi, Ni_2FeGa, and CoNiAl, *Acta Mater*., 2015, vol. 96, pp. 420–427. https://doi.org/10.1016/j.actamat.2015.06.011
5. Sutou, Y., Kamiya, N., Omori, T., Kainuma, R., Ishida, K., and Oikawa, K., Stress-Strain Characteristics in Ni-Fe-Ga Ferromagnetic Shape Memory Alloys, *Appl. Phys. Lett*., 2004, vol. 84, no. 8, pp. 1275–1277. https://doi.org/10.1063/1.1642277
6. Hamilton, R.F., Sehitoglu, H., Efstathiou, C., and Maier, H.J., Mechanical Response of NiFeGa Alloys Containing Second-Phase Particles, *Scripta Mater*., 2007, vol. 57, pp. 497–499. https://doi.org/10.1016/j.scriptamat.2007.05.024
7. Panchenko, E.Y., Yanushonite, E.I., Eftifeeva, A.S., Tokhmetova, A.B., Kurlevskaya, I.D., Tagiltsev, A.I., Surikov, N.S., Timofeeva, E.E., and Chumlyakov, Y.I., Elastocaloric Effect in Aged Single Crystals of $Ni_{54}Fe_{19}Ga_{27}$ Ferromagnetic Shape Memory Alloy, *Metals*, 2022, vol. 12, p. 1398. https://doi.org/10.3390/met12081398
8. Eftifeeva, A., Panchenko, E., Yanushonite, E., Kurlevskaya, I., Timofeeva, E., Tokhmetova, A., Surikov, N., Tagiltsev, A., and Chumlyakov, Y., Superelasticity and Elastocaloric Cooling Capacity in Stress-Induced Martensite Aged $[001]_A$-Oriented $Ni_{54}Fe_{19}Ga_{27}$ Single Crystals, *Mater. Sci. Eng. A*, 2022, vol. 855, p. 143855. https://doi.org/10.1016/j.msea.2022.143855
9. Surikov, N.Y., Panchenko, E.Y., and Chumlyakov, Y.I., The Elastocaloric Effect in [001]-Single Crystals of Titanium Nickelide Containing Nanosized Ti_3Ni_4 Particles, *Russ. Phys. J*., 2022, vol. 64, no. 9, pp. 1708–1714. https://doi.org/10.1007/s11182-022-02511-w
10. Dar, R.D., Yan, H., and Chen, Y., Grain Boundary Engineering of Co–Ni–Al, Cu–Zn–Al, and Cu–Al–Ni Shape Memory Alloys by Intergranular Precipitation of a Ductile Solid Solution Phase, *Scripta Mater*., 2016, vol. 115, pp. 113–117. https://doi.org/10.1016/j.scriptamat.2016.01.014
11. Ueland, S.M., Chen, Y., and Schuh, C.A., Oligocrystalline Shape Memory Alloys, *Adv. Funct. Mater*., 2012, vol. 22, pp. 2094–2099. https://doi.org/10.1002/adfm.201103019
12. Lee, J.S. and Wayman, C.M., Grain Refinement of Cu-Zn-Al Shape Memory Alloys, *Metallography*, 1986, vol. 19, pp. 401–419. https://doi.org/10.1016/0026-0800(86)90074-1
13. Zhang, X., Sui, J., Yu, Z., and Cai, W., Structure and Shape Memory Effect in a $Ni_{54}Mn_{25}Ga_{20}Gd_1$ Alloy with a High Transformation Temperature, *J. Alloys Compds*, 2011, vol. 509, pp. 8032–8037. https://doi.org/10.1016/j.jallcom.2011.04.144
14. Huang, X.-M., Zhao, Y., Yan, H.-L., Jia, N., Yang, B., Li, Z., Zhang, Y., Esling, C., Zhao, X., Ren, Q., Tong, X., and Zuo, L., Enhanced Cyclic Stability and Enlarged Working Temperature Window of NiFeGa Elastocaloric Refrigerant Via Introducing Strong Texture and Ductile Interfacial Precipitate, *Scripta Mater*., 2023, vol. 234, p. 115544. https://doi.org/10.1016/j.scriptamat.2023.115544
15. Imran, M., Zhang, X., Qian, M., and Geng, L., Enhanced Working Stability of Elastocaloric Effects in Polycrystalline Ni-Fe-Ga Dual Phase Alloy, *Intermetallics*, 2021, vol. 136, p. 107255. https://doi.org/10.1016/j.intermet.2021.107255
16. Oikawa, K., Omori, T., Sutou, Y., Morito, H., Kainuma, R., and Ishida, K., Phase Equilibria and Phase Transition of the Ni-Fe-Ga Ferromagnetic Shape Memory Alloy System, *Metallurg. Mater. Trans. A*, 2007, vol. 38, pp. 767–776. https://doi.org/10.1007/s11661-007-9095-8
17. Santamarta, R., Cesari, E., Font, J., Muntasell, J., Pons, J., and Dutkiewicz, J., Effect of Atomic Order on the Martensitic Transformation of Ni–Fe–Ga Alloys, *Scripta Mater*., 2006, vol. 54, no. 12, pp. 1985–1989. https://doi.org/10.1016/j.scriptamat.2006.03.018
18. Masdeu, F., Pons, J., Torrens-Serra, J., Chumlyakov, Y., and Cesari, E., Superelastic Behavior and Elastocaloric Effect in a $Ni_{51.5}Fe_{21.5}Ga_{27.0}$ Ferromagnetic Shape Memory Single Crystal under Compression,

Mater. Sci. Eng. A, 2022, vol. 833, p. 142362. https://doi.org/10.1016/j.msea.2021.142362

19. Zheng, H., Xia, M., Liu, J., Huang, Y., and Li, J., Martensitic Transformation of $(Ni_{55.3}Fe_{17.6}Ga_{27.1})_{100-x}Co_x$ Magnetic Shape Memory Alloys, *Acta Mater*., 2005, vol. 53, pp. 5125–5129. https://doi.org/10.1016/j.actamat.2005.07.023
20. Ortinh, J. and Planes, A., Thermodynamic Analysis of Thermal Measurements in Thermoelastic Martensitic Transformation, *Acta Metall*., 1988, vol. 36, pp. 1873–1889. https://doi.org/10.1016/0001-6160(88)90291-x
21. Beke, D.L., Daryczi, L., and Elrasasi, T.Y., Determination of Elastic and Dissipative Energy Contributions to Martensitic Phase Transformation in Shape Memory Alloys, in *Shape Memory Alloys—Processing, Characterization and Applications*, 2013, pp. 1–30. https://doi.org/10.5772/51511
22. Tusek, J., Engelbrecht, K., Mañosa, L., Vives, E., and Pryds, N., Understanding the Thermodynamic Properties of the Elastocaloric Effect through Experimentation and Modelling, *Shap. Mem. Superelasticity*, 2016, vol. 2, pp. 317–329. https://doi.org/10.1007/s40830-016-0094-8
23. Mañosa, L. and Planes, A., Materials with Giant Mechanocaloric Effects: Cooling by Strength, *Adv. Mater*., 2017, vol. 29, p. 1603607. https://doi.org/10.1002/adma.201603607
24. Xiao, F., Jin, M., Liu, J., and Jin, X., Elastocaloric Effect in Ni50Fe19Ga27Co4 Single Crystals, *Acta Mater*., 2015, vol. 96, pp. 292–300. http://dx.doi.org/10.1016/j.actamat.2015.05.054